Published in final edited form as:
Cell Rep. 2015 September 8; 12(10): 1691–1703. doi:10.1016/j.celrep.2015.07.064.

Telomerase Is Essential for Zebrafish Heart Regeneration

Dorota Bednarek[1], **Juan Manuel González-Rosa**[2,6,7], **Gabriela Guzmán-Martínez**[3], **Óscar Gutiérrez-Gutiérrez**[1], **Tania Aguado**[1], **Carlota Sánchez-Ferrer**[1], **Inês João Marques**[2], **María Galardi-Castilla**[2], **Irene de Diego**[1], **Manuel José Gómez**[4], **Alfonso Cortés**[5], **Agustín Zapata**[5], **Luis Jesús Jiménez-Borreguero**[3], **Nadia Mercader**[2,8,*], and **Ignacio Flores**[1,*]

[1]Regeneration and Aging Group, Centro Nacional de Investigaciones Cardiovasculares (CNIC-ISCIII), Melchor Fernández Almagro 3, 28029 Madrid, Spain

[2]Development of the Epicardium and Its Role during Regeneration Group, Centro Nacional de Investigaciones Cardiovasculares (CNIC-ISCIII), Melchor Fernández Almagro 3, 28029 Madrid, Spain

[3]Cardiovascular Imaging in Humans, Centro Nacional de Investigaciones Cardiovasculares (CNIC-ISCIII), Melchor Fernández Almagro 3, 28029 Madrid, Spain

[4]Bioinformatic Unit, Centro Nacional de Investigaciones Cardiovasculares (CNIC-ISCIII), Melchor Fernández Almagro 3, 28029 Madrid, Spain

[5]Electron Microscopy Center, Complutense University, Madrid 28040, Spain

SUMMARY

After myocardial infarction in humans, lost cardiomyocytes are replaced by an irreversible fibrotic scar. In contrast, zebrafish hearts efficiently regenerate after injury. Complete regeneration of the zebrafish heart is driven by the strong proliferation response of its cardiomyocytes to injury. Here we show that, after cardiac injury in zebrafish, telomerase becomes hyperactivated, and telomeres elongate transiently, preceding a peak of cardiomyocyte proliferation and full organ recovery. Using a telomerase-mutant zebrafish model, we found that telomerase loss drastically decreases cardiomyocyte proliferation and fibrotic tissue regression after cryoinjury and that cardiac function does not recover. The impaired cardiomyocyte proliferation response is accompanied by

*Correspondence: nmercader@cnic.es (N.M.), iflores@cnic.es (I.F.).
[6]Present address: Cardiovascular Research Center, Massachusetts General Hospital, Charlestown, MA 02129, USA
[7]Present address: Harvard Medical School, Boston, MA 02115, USA
[8]Present Address: Institute of Anatomy, University of Bern, Bern, Switzerland

AUTHOR CONTRIBUTIONS

D.B. performed laboratory-based experimental work, image acquisition, data quantification, data analysis, and telomere analysis. J.M.G.R. contributed to the experimental work. G.G. and J.J.B. performed and analyzed the echocardiography study. O.G.G. and T.A. and C.S.F performed the TRAP assay. I.J.M. performed the immunofluorescence analysis and cryoinjuries. M.G. contributed to the experiments with ex vivo cultures. I.D. performed experimental work. M.J.G. R. performed the transcriptome analysis. A.C. and A.Z. performed the TEM study. I.F., N.M., D.B., and J.M.G.R. designed the experiments and wrote the manuscript. I.F. directed the research.

ACCESSION NUMBERS

The accession number for the RNA-seq data reported in this paper is GSE71755.

SUPPLEMENTAL INFORMATION

Supplemental Information includes seven figures, one table, and six movies and can be found with this article online at http://dx.doi.org/10.1016/j.celrep.2015.07.064.

Europe PMC Funders Author Manuscripts

the absence of cardiomyocytes with long telomeres and an increased proportion of cardiomyocytes showing DNA damage and senescence characteristics. These findings demonstrate the importance of telomerase function in heart regeneration and highlight the potential of telomerase therapy as a means of stimulating cell proliferation upon myocardial infarction.

Graphical Abstract

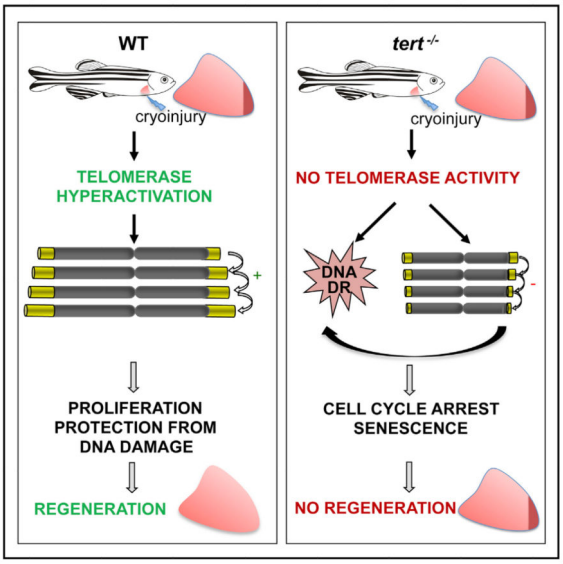

In Brief

Bednarek et al. find that telomerase, well known for its role in elongating telomere ends, is essential during zebrafish heart regeneration. Cardiac injury hyperactivates telomerase and increases telomere length in cardiac cells. In telomerase-null mutants, cardiac cells accumulate DNA damage and do not efficiently proliferate in response to injury.

INTRODUCTION

Heart disease is the leading cause of human death in the world. Currently, the only effective treatment for the loss of cardiomyocytes after infarction or heart failure is transplantation. Great hope has been placed on stem cell therapies, but, although data from clinical trials are promising, they fall far short of fulfilling expectations. This has led many researchers to consider taking a step back from the “bedside to the bench” before continuing with more clinical trials (Couzin-Frankel, 2014; Mummery and Lee, 2013). Understanding the repair mechanisms operating in vertebrates with a strong cardiac repair capacity may help to identify new molecules and pathways that could be used to promote heart regeneration in humans.

The zebrafish has become a powerful model for investigating regenerative processes because of its capacity to completely repair several organs, including the heart, after injury (Gemberling et al., 2013). The zebrafish heart can regenerate after ventricular resection (Poss et al., 2002; Raya et al., 2003), genetic ablation of cardiomyocytes (Wang et al.,

Europe PMC Funders Author Manuscripts

2011), hypoxia-reoxygenation injury (Parente et al., 2013), and ventricular cryoinjury (Chablais et al., 2011; González-Rosa et al., 2011; Schnabel et al., 2011). Cryoinjury causes local damage to all cardiac cell types and leads to a transient fibrotic tissue deposition reminiscent of the fibrotic scar formed in mammals after myocardial infarction (Chablais et al., 2011; González-Rosa et al., 2011). In the zebrafish, dead cardiomyocytes are replaced not by stem cells but by preexisting cardiomyocytes, which first dedifferentiate and then proliferate to replace the injured tissue with newly formed myocardium (Jopling et al., 2010; Kikuchi et al., 2010). This cardiomyocyte proliferation and remodeling requires paracrine-like contributions from the endocardial lining of the heart lumen and from the epicardium, the outer mesothelial layer covering the myocardium. Early after cardiac injury, the endocardium and epicardium start to re-express developmental genes (Kikuchi et al., 2011; Lepilina et al., 2006). One of these genes encodes retinaldehyde dehydrogenase aldh1a2, an enzyme involved in retinoic acid production that is proposed to be necessary for cardiomyocyte proliferation (Kikuchi et al., 2011). The endocardium also activates the expression of *il11a*, which triggers a jak1/stat3 signaling pathway in cardiomyocytes (Fang et al., 2013). In parallel, the epicardium starts to release extracellular matrix components such as fibronectin, which has been suggested to promote cardiomyocyte regeneration through interaction with integrin β 3 (itgβ3) (Wang et al., 2013).

A similar ability to proliferate in response to injury is shown by cardiomyocytes of neonatal mice (Porrello et al., 2011, 2013), and a limited degree of cardiomyocyte turnover has been reported in humans (Bergmann et al., 2009; Mollova et al., 2013). These observations suggest a new avenue for the treatment of heart failure based on enhancing the endogenous proliferation capacity of cardiomyocytes (Kikuchi and Poss, 2012; Takeuchi, 2014).

Successful DNA replication and extensive cell proliferation require the presence of functional telomeres, the capping structure at the end of chromosomes. Telomeres become shortened because of the end replication problem and other degradative activities (Saretzki and von Zglinicki, 2002). The ability of a cell to proliferate is therefore tightly linked to its ability to maintain healthy telomeres and avoid DNA damage. Telomerase is a ribonucleoprotein enzyme that maintains telomere length by adding DNA repeats to chromosome ends (Greider and Blackburn, 1985). Because of its ability to counteract telomere erosion, telomerase is associated with the proliferation potential of cells and tissues (Flores and Blasco, 2010; Flores et al., 2005) and has been implicated in mouse liver regeneration (Tümpel and Rudolph, 2012). Telomerase can be detected in zebrafish of all ages (Anchelin et al., 2011; Lund et al., 2009), and its expression level correlates with the life-long regenerative capacity of heart and fin tissues (Itou et al., 2012). In contrast, telomerase expression is suppressed rapidly postnatally in human and mouse tissues, with the exception of those with high turnover, reinforcing the association between telomerase activity and repair potential (Forsyth et al., 2002). Remarkably, human and zebrafish telomeres are of a similar size, making the zebrafish a good model for studying the contribution of telomere biology to regeneration (Henriques et al., 2013). Recent reports have described a zebrafish null mutant for the gene encoding telomerase reverse transcriptase (*tert*), the catalytic subunit of the telomerase enzyme (Anchelin et al., 2013; Henriques et al., 2013). Loss of *tert* leads to premature aging in several organs, including the

liver, intestine, and pancreas. However, the impact of loss of *tert* on zebrafish organ regeneration remains unexplored.

Here we analyzed the role of tert during zebrafish cardiac regeneration. We report that ventricular cryoinjury upregulates *tert* gene expression and telomerase activity in cardiac cells. In *tert*-null fish, cardiac regeneration is inhibited, and a fibrotic scar remains. This inability to regenerate is mainly due to a strong inhibition of the proliferation response associated with accumulation of cardiac cells with damaged DNA and senescence characteristics. These results highlight the potential of telomere restitution as an approach to reawakening hibernating myocardium after cardiac injury.

RESULTS

Zebrafish cardiomyocytes are able to proliferate throughout life (Itou et al., 2012) but markedly increase their proliferation index upon injury (Chablais et al., 2011; González-Rosa et al., 2011; Poss et al., 2002; Raya et al., 2003; Schnabel et al., 2011; Wang et al., 2011). Telomerase activity is linked to the ability of cells and tissues to proliferate (Flores and Blasco, 2010; Flores et al., 2005). We therefore first compared telomerase activity in zebrafish hearts under homeostatic conditions and during regeneration. A PCR-based telomerase activity assay revealed amplification bands in uninjured heart tissues from 6- to 9-month-old zebrafish, confirming telomerase activity in adults under homeostatic conditions (Figure 1A). There were no significant differences in telomerase activity between the hearts of 6- and 10-month-old fish (Figures 1B and 1C). Cryoinjury of the ventricular apex (one quarter of the ventricle) provoked a transient increase in the processivity and intensity of the amplification bands 3 days later, demonstrating that telomerase activity further increases in response to injury (Figure 1A). Injury-associated telomerase hyperactivation was accompanied by a 2.2-fold increase in *tert* gene expression 3 days postinjury (dpi), pointing to transcriptional activation as a likely regulation mechanism (Figure 1D).

To determine the relationship between telomerase hyperactivation and cardiac regeneration, we analyzed the regenerative capacity of a recently described zebrafish mutant line that carries a stop codon in the second exon of the *tert* gene (Anchelin et al., 2013; Henriques et al., 2013). This mutant completely lacks telomerase activity in the heart and can be considered a *tert* knockout (Figure 1E). Despite lacking telomerase activity, hearts from 6- to 9-month-old $tert^{-/-}$ fish are of normal size and show normal histology and cardiac function as measured by echocardiography (Figures 1F–1H). The lack of an obvious phenotype in $tert^{-/-}$ hearts at 6–9 months of age is consistent with the lack of phenotypic alterations in low-turnover $tert^{-/-}$ tissues at young ages (Anchelin et al., 2013; Henriques et al., 2013).

We next compared the regeneration response in wild-type (WT) and $tert^{-/-}$ zebrafish siblings subjected to heart cryoinjury. In both genotypes, we observed an obvious wound at the earliest time analyzed (3 dpi) (Figure 2A). The injured region was 20% ± 5% of the total ventricle in WT hearts and 21% ± 6% in $tert^{-/-}$ hearts. In WT hearts, the size of the wound decreased gradually, whereas a large wound persisted in $tert^{-/-}$ hearts at 60 dpi (Figures

2A–2C). Histological analysis in both genotypes confirmed the characteristic scar-like fibrotic tissue deposition triggered by cryoinjury (González-Rosa et al., 2011), but subsequent healing took place only in WT hearts (Figures 2B and 2C). The injured area at 60 dpi represented less than 5% of the ventricular area in WT hearts (2.5% ± 0.8%) but, in *tert*$^{-/-}$ hearts, was comparable with the injured area at 3 dpi (18% ± 2%; Figure 2C). To further substantiate the impaired regeneration response in *tert*$^{-/-}$ hearts, we evaluated cardiac function by 2D echocardiography (González-Rosa et al., 2014). Cryoinjury caused a reduction in systolic function at 7 dpi (measured by fractional volume shortening [FVS]) of 47% ± 8% in WT fish and 35% ± 4% in *tert*$^{-/-}$ fish (Figures 2D and 2E; Movies S1, S2, S3, S4, S5, and S6). FVS recovered gradually during regeneration in WT individuals, indicating reestablished ventricular function. In contrast, ventricular function did not recover in *tert*$^{-/-}$ animals, even at 60 dpi (Figures 2D and 2E; Movies S1, S2, S3, S4, S5, and S6). These results indicate that telomerase is required for heart regeneration in zebrafish.

Myocardial injury triggers a rapid inflammatory response, leading to the infiltration of the injury site by neutrophils, macrophages, and other circulating cells (Frangogiannis, 2014). This inflammatory response, particularly the infiltration of macrophages, plays a key role in promoting cardiac regeneration in the neonatal mouse heart (Aurora et al., 2014). Given that gene silencing of *tert* has been shown to impair hematopoiesis (Imamura et al., 2008), we assessed whether *tert*$^{-/-}$ zebrafish show alterations in cryoinjury-triggered inflammation. Whole-heart RNA sequencing (RNA-seq) analysis did not detect significant differences between the upregulation of neutrophil, macrophage, and other inflammatory cell markers in *tert*$^{-/-}$ and wild-type hearts at 3 dpi (Figure S1A; Table S1). In addition, L-plastin immunohistochemistry at 3 and 60 dpi revealed no significant differences in macrophage infiltration (Figures S1B–S1G).

The dedifferentiation and proliferation of pre-existing cardiomyocytes during zebrafish heart regeneration is preceded by rapid and organ-wide activation of the endocardium and epicardium (Kikuchi et al., 2011; Lepilina et al., 2006). To determine whether the absence of telomerase activity alters the activation of endocardium and epicardium, we analyzed the expression of *aldh1a2* (*raldh2*) (Kikuchi et al., 2011). WT and *tert*$^{-/-}$ animals showed a similarly strong upregulation of *aldh1a2* RNA and protein in endocardial cells at 6 hr postinjury (hpi) and in endocardial and epicardial cells at 3 dpi (Figure S2A). These results were confirmed by RNA-seq (Figure S2B) and qRT-PCR (data not shown). We also tested the expression of another endocardial gene (*il11a*) and epicardial genes (*wt1b, tbx18*, and *fibronectin)* upregulated upon cardiac injury (Fang et al., 2013; Kikuchi et al., 2011; Lepilina et al., 2006), finding no alterations in their expression in injured *tert*$^{-/-}$ hearts (Figure S2B). The early injury responses of the epicardium and endocardium are therefore not affected in the absence of telomerase.

In response to injury, cardiomyocyte sarcomeres disassemble, mitochondria swell, and cellular attachments loosen (Jopling et al., 2010; Kikuchi et al., 2010). To determine whether these signs of cardiomyocyte dedifferentiation are affected by the loss of telomerase, we analyzed cardiomyocyte ultrastructural features at 3 dpi by transmission electron microscopy. A similar extent of sarcomere disassembly and mitochondrial swelling and dysmorphia was detected in WT and *tert*$^{-/-}$ cardiomyocytes close to the injury site

(Figure S3), indicating that cardiomyocyte dedifferentiation proceeds normally in the absence of telomerase.

After dedifferentiation, cardiomyocytes proliferate. To study the proliferation response in WT and *tert*$^{-/-}$ animals, we examined the percentage of cardiac cells positive for proliferating cell nuclear antigen (PCNA), a marker of cells in S phase (Figures 3A–3C). A sharp peak in proliferation occurred at 3 dpi in WT hearts, affecting ~11% of total cardiac cells. In *tert*$^{-/-}$ hearts, the proliferation peak was delayed to 14 dpi and affected a maximum of ~6% of cardiac cells (Figure 3A). The impairment in the proliferation response was more pronounced for the cardiomyocyte pool, where the proliferation peak at 7 dpi was 3-fold lower in *tert* $^{-/-}$ hearts (Figure 3B). Proliferating cardiomyocytes in WT hearts were found predominantly at the injury borders but were also detected in peripheral regions (Figure 3C). In *tert*$^{-/-}$ hearts, a weakened proliferation response was evident at all analyzed stages both at the injury border zone and at the periphery (Figure 3C). Interestingly, the few proliferating cardiomyocytes in *tert*$^{-/-}$ hearts were mainly localized close to the epicardium at 60 dpi (Figure 3C). To further characterize the impaired proliferation capacity, we labeled hearts with bromodeoxyuridine (BrdU) to assess DNA synthesis and stained sections with antibodies against BrdU and the mitosis marker phosphorylated histone H3 (pH3). For both markers, we observed large relative reductions in the number of positive cells in *tert*$^{-/-}$ hearts (Figures 3D and 3E; Figure S4A). These results indicate that the failure of cardiac regeneration in the absence of telomerase is due to an impaired proliferation response of cardiomyocytes and other cardiac cells. Gene set enrichment analysis (GSEA) confirmed that cell proliferation-associated pathways were impaired significantly in *tert*$^{-/-}$ hearts compared with the WT (Table S1; Figure S4B).

To dissect the temporal and spatial action of tert during cardiac cell proliferation, we injured hearts ex vivo and examined the effect of tert-targeting vivo antisense Morpholino oligonucleotides (vivoMO). After culture ex vivo for 3 days, untreated injured hearts contained PCNA-positive cardiac cells, including cardiomyocytes, in the peripheral borders of the ventricle. Incubation with *tert* vivoMO during ex vivo culture markedly reduced telomerase activity and the number of PCNA-positive cells (Figures S5A–S5C). Similar results were obtained for the proliferation marker pH3 (data not shown). These data support the conclusion that tert function is necessary for cardiac cell proliferation in the adult heart during cardiac regeneration.

We next investigated how telomerase influences proliferation. Because the canonical function of telomerase is to lengthen telomeres, and long telomeres provide proliferation potential, we conducted telomapping assays to determine whether telomerase hyperactivation leads to changes in telomere length during heart regeneration (Flores et al., 2008). Measurement of average telomere length in each cell on sections of whole WT hearts showed that cardiac telomeres elongate transiently during heart regeneration, with a peak of lengthening at 3 dpi (Figures 4A and 4B). Telomere elongation was detected in cardiomyocytes and other cell types, including endocardial cells (Figure S6). In contrast, telomere length in *tert*$^{-/-}$ hearts decreased after cryoinjury, reaching half the initial length at 60 dpi (Figure 4B).

Given that telomere length is linked to proliferation potential in several organs, we next compared the telomere length of proliferative and non-proliferative cardiac cells. Single-cell profiling of telomere length and analysis of PCNA expression revealed that proliferating WT cardiac cells possess longer telomeres than non-proliferative cells, indicating that, in WT fish, telomere length defines a subclass of cardiac cells with proliferation potential (Figure 5A). During regeneration, telomeres lengthened not only in actively proliferating cells but also in non-proliferating cells, demonstrating that telomere elongation is a general process within the regenerating heart (Figure 5A). To determine the location of proliferative cardiomyocytes and their telomere length, we co-immunostained sections for myosin heavy chain (MHC), PCNA, and telomeres. In uninjured WT hearts, cardiomyocyte telomere length is heterogeneous, with telomeres longer in proliferating cells (Figure 5B; Figure S6). After injury, the number of proliferating cardiomyocytes with long telomeres (>600 a.u.) increased to a peak at 7 dpi but then declined gradually. Therefore, despite telomerase hyperactivation after cryoinjury, telomerase activity levels are insufficient to maintain telomere reserves in cardiomyocytes (Figure 5B). The successive rounds of cell division taking place during regeneration are likely to contribute to telomere erosion. Consistent with this idea, telomeres shortened abruptly in cells close to the injury, the region with the highest proliferation rate (Figure S6). A similar pattern of rapid telomere erosion was observed in regions of the epicardium and endocardium adjacent to the injury site (Figure S6).

Short and dysfunctional telomeres limit cellular proliferative capacity by eliciting a DNA damage response. To assess the levels of DNA damage before and after injury in WT and *tert*$^{-/-}$ hearts, we measured the protein levels of the DNA damage marker phospho-histone H2A.X (γH2AX) (Rogakou et al., 1998; Figure 6). Cryoinjury increased the γH2AX signal in WT and *tert*$^{-/-}$ hearts, but the increase was significant only in *tert*$^{-/-}$ hearts (Figures 6A and 6B). DNA damage in cardiac cells was spread globally in the ventricles of non-injured WT hearts, and the number of damaged cells was not increased significantly after injury (Figures 6C and 6E). In contrast, *tert*$^{-/-}$ hearts contained higher basal numbers of γH2AX-positive cells, and the level of damage increased significantly after injury (Figures 6C and 6E). The same pattern was seen when only cardiomyocytes were examined (Figure 6F). The DNA damage response limits cellular proliferative capacity (Behrens et al., 2014). Consistent with this notion, co-immunostaining of the γH2AX and BrdU labels revealed that the vast majority of BrdU-positive cells were γH2AX-negative in both WT and *tert*$^{-/-}$ hearts (Figure S7). These results indicate that the absence of telomerase is an important contributor to DNA damage, with a likely impact on cardiac regeneration.

Telomere dysfunction-induced DNA damage and cell-cycle blockade can lead to cellular senescence (d'Adda di Fagagna et al., 2003). We therefore used the senescence-associated β-galactosidase assay to detect senescence in *tert*$^{-/-}$ hearts (Figure 7). Uninjured hearts of WT or *tert*$^{-/-}$ animals did not show senescence-specific staining, but a senescence-associated β-galactosidase signal was induced upon cryoinjury. In WT hearts at 3 dpi, senescent cells were almost exclusively limited to the injured region, whereas, in injured *tert*$^{-/-}$ hearts, the signal was distributed more broadly, extending beyond the injured area and border zone to remote regions of the ventricle, consistent with the organ-wide deficit of

proliferating *tert*$^{-/-}$ cardiac cells (Figure 7). This tendency was maintained at later stages of regeneration (7 dpi) (Figure 7).

DISCUSSION

Our results indicate that, under the high demands imposed by heart injury, telomere reserves cannot be maintained without telomerase. Absence of telomerase decouples dedifferentiation from proliferation, drastically impairing proliferation and leading to the accumulation of DNA damage. Instead of regenerating myocardium and regressing cardiac fibrosis, *tert*$^{-/-}$ hearts acquire a senescent phenotype. The telomere elongation and DNA protection roles of telomerase might be linked, and senescence could be the final outcome of DNA damage accumulation. The detection of mildly elevated DNA damage in the uninjured *tert*$^{-/-}$ heart might indicate that tert also maintains DNA during homeostasis, perhaps by protecting against oxidative or mechanical stress (Oh et al., 2003). Although this does not seem to impact basal cardiac function, it might contribute to the impaired regeneration observed in *tert*$^{-/-}$ mutant hearts.

In humans, telomerase is downregulated rapidly after birth (Wright et al., 1996). Interestingly, after an ischemic episode, cardiomyocytes can enter a state of hibernation in which viability is maintained but the myocardium is non-functional. This hibernating myocardium has been suggested to represent a partially dedifferentiated state (Heusch, 2004). Given the essential role of telomerase in cardiomyocyte expansion after dedifferentiation, our results highlight the potential of telomere restitution as a strategy to reawaken hibernating myocardium in the post-infarction heart.

EXPERIMENTAL PROCEDURES

Zebrafish Husbandry

All experiments were conducted with adult zebrafish between 6 and 9 months of age, raised at a density of 3 fish/l. Animals were housed and experiments were performed in accordance with Spanish bioethical regulations for the use of laboratory animals. The ethics committee that approved this study was the Community of Madrid “Dirección General de Medio Ambiente.” The telomerase *tert*$^{AB/hu3430}$ mutant line used in this study is available from the Zebrafish Model Organism Database (ZFIN) repository (ZFIN: ZDB-GENO-100412-50) at the Zebrafish International Resource Center (ZIRC). The *tert*$^{AB/hu3430}$ mutants have a T→A point mutation in the *tert* gene. Genotyping was performed by PCR of the *tert* gene (*tert* primers were as follows: forward, 5′GACGACCAGTTCGGATCCCTTC 3′; reverse, 5′ CTTTACCCTCCGCCGCTTTACC 3′). Characterization of *tert*$^{-/-}$ zebrafish was performed in F1 and F2 animals produced by *tert*$^{+/-}$ incrossing.

Cryoinjury

Cryoinjury was performed as described previously (González-Rosa and Mercader, 2012). For analysis of regeneration, animals were euthanized at different times post-injury by immersion in 0.16% tricaine (Sigma), and hearts were dissected in medium containing 2 U/ml heparin and 0.1 M KCl. The damaged area was easily identified from the accumulation of blood at the injury site. Damage was also estimated by examination of sections (Poss et

Europe PMC Funders Author Manuscripts

al., 2002). The percentage of the ventricular surface area damaged by the procedure was calculated using NIS-Elements AR, 64 bit 3.00, SP7 (Build 547).

Telomerase Assay

Telomerase activity was measured with a modified fluorescence telomere repeat amplification assay (Herbert et al., 2006).

Histological Staining

Hearts were fixed overnight at 4°C in 4% paraformaldehyde (PFA) in PBS. Samples were then washed in PBS + 0.1% Tween 20, dehydrated through an ethanol series, and embedded in paraffin wax. All histology was performed on 7-μm paraffin sections cut on a microtome (Leica), mounted on Superfrost slides (Fisher Scientific), and dried overnight at 37°C. Sections were deparaffinized in xylol, rehydrated, and washed in distilled water. Connective tissue was stained using the Masson-Goldner trichrome procedure (Merck).

Cardiac Imaging by Echocardiography

To assess cardiac function in non-injured and post-injury zebrafish, animals were anesthetized with a mixture of tricaine (130 ppm) and isoflurane (200 ppm) diluted in tank water (Huang et al., 2010). Individuals were then placed ventral side up in a custom-made sponge holder in a Petri dish filled with the anesthetic solution. 2D, high-resolution, real-time in vivo images were obtained with the Vevo770 imaging system through an RMV708 (22–83 MHz) scanhead (VisualSonics). Echocardiographic evaluation of heart size was performed by comparing ventricular volume measured in diastole between WT and *tert*$^{-/-}$ animals (González-Rosa et al., 2014).

In Situ Hybridization on Sections

In situ hybridization on paraffin sections was performed according to Mallo et al. (2000) with some modifications.

RNA-Seq Library Production

Index-tagged cDNA libraries were constructed from total RNA (1 μg) with the TruSeq RNA sample preparation v2 kit (Illumina). Four biological replicates consisting of three pooled hearts were used per sample. Quality, quantity, and size distribution of the Illumina libraries were determined using the DNA-1000 kit (Agilent Bioanalyzer). Libraries were sequenced (single-end mode and length of 75 bp) on the Genome Analyzer IIx system using the standard RNA sequencing protocol in the TruSeq SBS kit v5. Fastq files containing reads for each library were extracted and demultiplexed using Casava v1.8.2 pipeline.

RNA-Seq Analysis

Sequencing adaptor contaminations were removed from reads using Cutadapt software (Martin, 2011), and the resulting reads were mapped and quantified on the transcriptome (Ensembl gene-build 66) using RSEM v1.2.3 (Li and Dewey, 2011). Only genes with at least two counts per million in at least four samples were considered for statistical analysis. Data were then normalized, and deferential expression was tested using the bioconductor

package EdgeR (Robinson et al., 2010). We considered as differentially expressed genes with a Benjamini-Hochberg-adjusted p value of less than 0.05.

Electron Microscopy

Transmission electron microscopy was performed as described previously (Willett et al., 1999). Briefly, hearts were fixed in 2.5% glutaraldehyde/0.1 M sodium caccodylate at 4°C and post-fixed with 1% osmium tetroxide/0.1 M sodium caccodylate. After washing in 0.1 M sodium caccodylate/5% sucrose, the hearts were dehydrated quickly in increasing concentrations of ethanol to 100%. Hearts were then washed twice with propylene oxide and replaced with a 2:1 mixture of propylene oxide:PB 812 (PolySciences), then a 1:1 mixture of the same components, and, finally, with pure PB 812. Blocks were polymerized at 70°C overnight in fresh PB 812. Ultra-thin sections were double-stained with uranyl acetate and lead citrate, examined, and photographed in a JEOL 10.10 electron microscope.

Q-FISH Telomere Length Analysis on Zebrafish Heart Sections

Telomere quantitative fluorescence in situ hybridization (Q-FISH) analysis on paraffin-embedded sections was performed as described previously (Flores et al., 2008). Images were acquired with an A1R-A1 Nikon confocal microscope fitted with a 603 objective. Quantitative image analysis was performed on confocal images using Metamorph version 7 (Molecular Devices) as described previously (Flores et al., 2008). Briefly, the 4′,6-diamidino-2-phenylindole (DAPI) image was used to define the nuclear area and the Cy3 image to quantify telomere fluorescence. Telomere fluorescence intensity was measured as “average gray value” (total gray value per nucleus area). These “average telomere fluorescence” values represent the average Cy3 pixel intensity for the total nuclear area, thereby ruling out any influence of nuclear size on telomere length measurements. Telomere fluorescence values for each sample were exported to Microsoft Excel to generate frequency histograms. A four-color intensity banding was used to generate the map of telomere length. The injury area, determined by the absence of MHC staining, was excluded from the analysis.

Immunofluorescence

Heart sections were deparaffinized, rehydrated, and washed in distilled water. Epitopes were retrieved by heating in citrate buffer (pH 6.0) for 15 min in a microwave at full power. Non-specific binding sites were saturated by incubation for 1 hr in blocking solution (3% BSA, 5% goat serum, and 0.3% Tween 20). Endogenous biotin was blocked with the avidin-biotin blocking kit (Vector Laboratories). Slides were then incubated overnight with primary antibodies at 4°C. The primary antibodies used were anti-myosin heavy chain (MF20, Developmental Studies Hybridoma Bank [DSHB], diluted 1:20), anti-tropomyosin (CH1, DSHB, diluted 1:20), anti-L-plastin (provided by P. Martin, University of Bristol; Evans et al., 2013), anti-erg1 (Abcam, diluted 1:100), anti- PCNA (Santa Cruz Biotechnology, diluted 1:100), anti- BrdU (BD Biosciences, diluted 1:30), anti-pH3 (Millipore, diluted 1:100), and anti-γ-H2AX (GeneTex, diluted 1:300). The primary antibody signal was revealed after incubation for 1 hr at room temperature with biotin- or Alexa 488-, 568-, or 633conjugated secondary antibodies (Invitrogen, each diluted 1:200) and streptavidin-Cy5 (Vector). Nuclei were stained with DAPI (1:1,000), and slides were mounted in Vectashield (Vector).

Apoptosis was detected by terminal deoxynucleotidyl transferase dUTP nick end labeling (TUNEL) staining using the in situ cell death detection kit from Roche.

For combined analysis by Q-FISH and immunostaining for proliferation, we performed an additional step with the Vectastain Elite ABC standard kit (Vector) and the Cy5-conjugated Tyramide Signal Amplification Plus kit (TSA Plus, PerkinElmer). Endogenous peroxidase activities were quenched in 3% H_2O_2 in PBS for 10 min at room temperature. Before applying secondary antibodies, sections were incubated for 30 min with Vectastain Elite ABC reagent at room temperature. After three washes of 5 min each in PBS, slides were incubated for 4 min in tyramide-Cy5 conjugate diluted 1:100 in 1× Plus amplification diluent (PerkinElmer). After three additional 5-min washes, secondary antibodies were applied and slides were processed according to the immunofluorescence and Q-FISH procedure described above.

To quantify cardiomyocyte proliferation, three to six sections showing the largest wounds were selected from each heart, and images were obtained with a 60× objective to generate a tiled composite of the whole heart section. The cells positive for MHC and PCNA were counted manually in all ventricles. The percentages of MHC^+PCNA^+ cells from selected sections were averaged to determine a proliferation index for each heart.

BrdU Labeling

Animals were anesthetized in tricaine, and a single dose of BrdU (Sigma, 0.05 ml of 2.5 mg/ml solution dissolved in PBS) was injected intraperitoneally at 3 or 7 dpi. Animals were then left to continue healing until 7 or 14 dpi, respectively.

Imaging

Whole-heart images were obtained with a Leica MZ16FA fluorescence stereomicroscope fitted with a Leica DFC310FX camera. A Nikon Eclipse 90i microscope was used to examine histological and immunohistochemical staining, and a Nikon A1R confocal microscope was used for immunofluorescence staining.

Western Blot Analysis

Hearts were dissected and lysed in radioimmunoprecipitation assay (RIPA) buffer (50 mM Tris [pH 8], 150 mM NaCl, 0.1% SDS, 1% NP40, and 0.5% sodium deoxycholate) containing protease inhibitor cocktail (Roche). Total proteins (100 μg) were separated by SDS-PAGE and transferred to a polyvinylidene fluoride (PVDF) membrane. Blots were incubated overnight with primary antibodies. Anti-histone γH2AX (GeneTex, catalog no. GTX127342) was used at 1:1,000 dilution and α-tubulin (Sigma, catalog no. T8203) at 1:4,000 dilution. Horseradish peroxidase-coupled secondary antibodies (Dako) were used at 1:5,000 dilution. Band intensities were quantified densitometrically using QuantityOne software (BioRad).

Quantification of Phosphorylated H2AX Foci

Phosphorylated H2AX foci were detected with rabbit polyclonal anti-phospho-histone H2AX antibody (1:300, GeneTex). A cell was considered positive for γ-H2AX when it contained two or more foci. Foci were counted manually.

Senescence-Associated β-Galactosidase Activity

Senescence-associated β-galactosidase (SA β-gal) activity was detected on freshly prepared cryosections and whole-mounts using a senescence β-galactosidase staining kit (Cell Signaling Technology).

Vivo Morpholino Treatment of Ex Vivo-Cultured Hearts

Hearts were dissected from adult WT, Tg(*fli:GFP*) (Lawson and Weinstein, 2002), or Tg(*myl7:GFP*) (Raya et al., 2003) zebrafish in the *AB* genetic background. The apex was injured by stabbing with a tungsten needle. Stabbing was used because this method is less invasive than cryoinjury and, therefore, better supports survival in vitro while being equally well suited to the study of the cardiomyocyte proliferation response to injury (Itou et al., 2014). Hearts were cultured in DMEM supplemented with 10% fetal bovine serum and antibiotics (penicillin and streptomycin) in 96-well plates (Pieperhoff et al., 2014). Two hearts were added per well in 250 μl medium. The vivoMOs used were *tert* vivoMO (5′-CTGTCGAGTACTGTCCAGACATCTG; Imamura et al., 2008) and *gfp* vivoMO (5′-ACAGCTCCTCGCCCTTGCTCACCAT; Huang et al., 2003). All Morpholinos were added at a concentration of 10–15 μM. The medium was changed daily. After 3 days, hearts were either processed for the tert activity assay or fixed for sectioning and immunofluorescence. MO specificity was confirmed by injecting *tert* MOs into $tert^{-/-}$ embryos without causing any additional obvious phenotypes (data not shown).

Statistical Analysis

Where normal distribution can be assumed, Student’s t test for comparisons between two groups or one-way ANOVA followed by Tukey’s honest significance test for comparisons between more than two groups were used. Where the normality assumption could not be verified with a reliable method, Mann-Whitney test was used. Model assumptions of normality and homogeneity were checked with conventional residual plots. To control for the false discovery rate in RNA-seq data, p values were corrected for multiple testing using the Benjamini-Hochberg method (Benjamini and Hochberg, 1995), yielding adjusted p values. The specific test used in each comparison is indicated in the main text or figure legend. Calculations were made with Microsoft Excel version 14.4.9 and Prism version 5.0.

Supplementary Material

Refer to Web version on PubMed Central for supplementary material.

ACKNOWLEDGMENTS

We thank E. Díaz, R. Costa, R. Doohan, and A. de Molina for zebrafish husbandry and technical support; E. Arza and A. M. Santos for help with microscopy acquisition; F. Sánchez-Cabo and C. Torroja for help with statistics; and S. Bartlett for text editing. We are very grateful to M.L. Cayuela (Hospital Virgen de Arritxaca, Murcia, Spain) and

M.G. Ferreira (Instituto Gulbenkian de Ciência, Lisbon, Portugal) for sharing unpublished results, fish lines, and insightful discussions. The CNIC is supported by the Ministerio de Economia y Competitividad (MINECO) and the Pro-CNIC Foundation. This work was funded by grants from MINECO (SAF2012-38449 [to I.F.] and BFU2011-25297, Cardiocell, and FIBROTEAM S2010/BMD-2321 [to N.M.]), the Red Temática de Investigación Cooperativa en Enfermedades Cardiovasculares (RD12/0042/0045 [to I.F.]), and the ERC (ERC starting grant 337703–zebra-Heart [to N.M]). I.J.M is supported by PIEF-GA-2012-330728. D.B. is supported by FPI fellowship BES2010-033554 from MINECO.

REFERENCES

Anchelin M, Murcia L, Alcaraz-Pérez F, García-Navarro EM, Cayuela ML. Behaviour of telomere and telomerase during aging and regeneration in zebrafish. PloS ONE. 2011; 6:e16955. [PubMed: 21347393]

Anchelin M, Alcaraz-Pérez F, Martínez CM, Bernabé-García M, Mulero V, Cayuela ML. Premature aging in telomerase-deficient zebra-fish. Dis. Model Mech. 2013; 6:1101–1112. [PubMed: 23744274]

Aurora AB, Porrello ER, Tan W, Mahmoud AI, Hill JA, Bassel-Duby R, Sadek HA, Olson EN. Macrophages are required for neonatal heart regeneration. J. Clin. Invest. 2014; 124:1382–1392. [PubMed: 24569380]

Behrens A, van Deursen JM, Rudolph KL, Schumacher B. Impact of genomic damage and ageing on stem cell function. Nat. Cell Biol. 2014; 16:201–207. [PubMed: 24576896]

Benjamini Y, Hochberg Y. Controlling the false discovery rate: a practical and powerful approach to multiple testing. J. R. Stat. Soc. Series B Stat. Methodol. 1995; 57:289–300.

Bergmann O, Bhardwaj RD, Bernard S, Zdunek S, Barnabé-Heider F, Walsh S, Zupicich J, Alkass K, Buchholz BA, Druid H, et al. Evidence for cardiomyocyte renewal in humans. Science. 2009; 324:98–102. [PubMed: 19342590]

Chablais F, Veit J, Rainer G, Jaźwińska A. The zebrafish heart regenerates after cryoinjury-induced myocardial infarction. BMC Dev. Biol. 2011; 11:21. [PubMed: 21473762]

Couzin-Frankel J. The elusive heart fix. Science. 2014; 345:252–257. [PubMed: 25035469]

d'Adda di Fagagna F, Reaper PM, Clay-Farrace L, Fiegler H, Carr P, Von Zglinicki T, Saretzki G, Carter NP, Jackson SP. A DNA damage checkpoint response in telomere-initiated senescence. Nature. 2003; 426:194–198. [PubMed: 14608368]

Evans MA, Smart N, Dubé KN, Bollini S, Clark JE, Evans HG, Taams LS, Richardson R, Lévesque M, Martin P, et al. Thymosin β4-sulfoxide attenuates inflammatory cell infiltration and promotes cardiac wound healing. Nat. Commun. 2013; 4:2081. [PubMed: 23820300]

Fang Y, Gupta V, Karra R, Holdway JE, Kikuchi K, Poss KD. Translational profiling of cardiomyocytes identifies an early Jak1/Stat3 injury response required for zebrafish heart regeneration. Proc. Natl. Acad. Sci. U.S.A. 2013; 110:13416–13421. [PubMed: 23901114]

Flores I, Blasco MA. The role of telomeres and telomerase in stem cell aging. FEBS Lett. 2010; 584:3826–3830. [PubMed: 20674573]

Flores I, Cayuela ML, Blasco MA. Effects of telomerase and telomere length on epidermal stem cell behavior. Science. 2005; 309:1253–1256. [PubMed: 16037417]

Flores I, Canela A, Vera E, Tejera A, Cotsarelis G, Blasco MA. The longest telomeres: a general signature of adult stem cell compartments. Genes Dev. 2008; 22:654–667. [PubMed: 18283121]

Forsyth NR, Wright WE, Shay JW. Telomerase and differentiation in multicellular organisms: turn it off, turn it on, and turn it off again. Differentiation. 2002; 69:188–197. [PubMed: 11841477]

Frangogiannis NG. The inflammatory response in myocardial injury, repair, and remodelling. Nat. Rev. Cardiol. 2014; 11:255–265. [PubMed: 24663091]

Gemberling M, Bailey TJ, Hyde DR, Poss KD. The zebrafish as a model for complex tissue regeneration. Trends Genet. 2013; 29:611–620. [PubMed: 23927865]

González-Rosa JM, Mercader N. Cryoinjury as a myocardial infarction model for the study of cardiac regeneration in the zebrafish. Nat. Protoc. 2012; 7:782–788. [PubMed: 22461067]

González-Rosa JM, Martín V, Peralta M, Torres M, Mercader N. Extensive scar formation and regression during heart regeneration after cryoinjury in zebrafish. Development. 2011; 138:1663–1674. [PubMed: 21429987]

González-Rosa JM, Guzmán-Martínez G, Marques IJ, Sánchez-Iranzo H, Jiménez-Borreguero LJ, Mercader N. Use of echocardiography reveals reestablishment of ventricular pumping efficiency and partial ventricular wall motion recovery upon ventricular cryoinjury in the zebrafish. PLoS ONE. 2014; 9:e115604. [PubMed: 25532015]

Greider CW, Blackburn EH. Identification of a specific telomere terminal transferase activity in Tetrahymena extracts. Cell. 1985; 43:405–413. [PubMed: 3907856]

Henriques CM, Carneiro MC, Tenente IM, Jacinto A, Ferreira MG. Telomerase is required for zebrafish lifespan. PLoS Genet. 2013; 9:e1003214. [PubMed: 23349637]

Herbert B-S, Hochreiter AE, Wright WE, Shay JW. Nonradioactive detection of telomerase activity using the telomeric repeat amplification protocol. Nat. Protoc. 2006; 1:1583–1590. [PubMed: 17406450]

Heusch G. Myocardial hibernation: a delicate balance. Am. J. Physiol. Heart Circ. Physiol. 2004; 288:H984–H999. [PubMed: 15563526]

Huang CJ, Tu CT, Hsiao CD, Hsieh FJ, Tsai HJ. Germ-line transmission of a myocardium-specific GFP transgene reveals critical regulatory elements in the cardiac myosin light chain 2 promoter of zebrafish. Dev. Dyn. 2003; 228:30–40. [PubMed: 12950077]

Huang WC, Hsieh YS, Chen IH, Wang CH, Chang HW, Yang CC, Ku TH, Yeh SR, Chuang YJ. Combined use of MS-222 (tricaine) and isoflurane extends anesthesia time and minimizes cardiac rhythm side effects in adult zebrafish. Zebrafish. 2010; 7:297–304. [PubMed: 20807039]

Imamura S, Uchiyama J, Koshimizu E, Hanai J, Raftopoulou C, Murphey RD, Bayliss PE, Imai Y, Burns CE, Masutomi K, et al. A non-canonical function of zebrafish telomerase reverse transcriptase is required for developmental hematopoiesis. PLoS ONE. 2008; 3:e3364. [PubMed: 18846223]

Itou J, Kawakami H, Burgoyne T, Kawakami Y. Life-long preservation of the regenerative capacity in the fin and heart in zebrafish. Biol. Open. 2012; 1:739–746. [PubMed: 23213467]

Itou J, Akiyama R, Pehoski S, Yu X, Kawakami H, Kawakami Y. Regenerative responses after mild heart injuries for cardiomyocyte proliferation in zebrafish. Dev. Dyn. 2014; 243:1477–1486. [PubMed: 25074230]

Jopling C, Sleep E, Raya M, Martí M, Raya A, Izpisua Belmonte JC. Zebrafish heart regeneration occurs by cardiomyocyte dedifferentiation and proliferation. Nature. 2010; 464:606–609. [PubMed: 20336145]

Kikuchi K, Poss KD. Cardiac regenerative capacity and mechanisms. Annu. Rev. Cell Dev. Biol. 2012; 28:719–741. [PubMed: 23057748]

Kikuchi K, Holdway JE, Werdich AA, Anderson RM, Fang Y, Egnaczyk GF, Evans T, MacRae CA, Stainier DYR, Poss KD. Primary contribution to zebrafish heart regeneration by gata4+ cardiomyocytes. Nature. 2010; 464:601–605. [PubMed: 20336144]

Kikuchi K, Holdway JE, Major RJ, Blum N, Dahn RD, Begemann G, Poss KD. Retinoic acid production by endocardium and epicardium is an injury response essential for zebrafish heart regeneration. Dev. Cell. 2011; 20:397–404. [PubMed: 21397850]

Lawson ND, Weinstein BM. In vivo imaging of embryonic vascular development using transgenic zebrafish. Dev. Biol. 2002; 248:307–318. [PubMed: 12167406]

Lepilina A, Coon AN, Kikuchi K, Holdway JE, Roberts RW, Burns CG, Poss KD. A dynamic epicardial injury response supports progenitor cell activity during zebrafish heart regeneration. Cell. 2006; 127:607–619. [PubMed: 17081981]

Li B, Dewey CN. RSEM: accurate transcript quantification from RNA-Seq data with or without a reference genome. BMC Bioinformatics. 2011; 12:323. [PubMed: 21816040]

Lund TC, Glass TJ, Tolar J, Blazar BR. Expression of telomerase and telomere length are unaffected by either age or limb regeneration in Danio rerio. PloS ONE. 2009; 4:e7688. [PubMed: 19893630]

Mallo M, Schrewe H, Martin JF, Olson EN, Ohnemus S. Assembling a functional tympanic membrane: signals from the external acoustic meatus coordinate development of the malleal manubrium. Development. 2000; 127:4127–4136. [PubMed: 10976045]

Martin M. Cutadapt removes adapter sequences from high-throughput sequencing reads. EMBnet J. 2011; 17:10–12.

Mollova M, Bersell K, Walsh S, Savla J, Das LT, Park S-Y, Silberstein LE, dos Remedios CG, Graham D, Colan S, et al. Cardiomyocyte proliferation contributes to heart growth in young humans. Proc. Natl. Acad. Sci. U.S.A. 2013; 110:1446–1451. [PubMed: 23302686]

Mummery CL, Lee RT. Is heart regeneration on the right track? Nat. Med. 2013; 19:412–413. [PubMed: 23558629]

Oh H, Wang SC, Prahash A, Sano M, Moravec CS, Taffet GE, Michael LH, Youker KA, Entman ML, Schneider MD. Telo-mere attrition and Chk2 activation in human heart failure. Proc. Natl. Acad. Sci. U.S.A. 2003; 100:5378–5383. [PubMed: 12702777]

Parente V, Balasso S, Pompilio G, Verduci L, Colombo GI, Milano G, Guerrini U, Squadroni L, Cotelli F, Pozzoli O, et al. Hypoxia/reoxygenation cardiac injury and regeneration in zebrafish adult heart. PloS ONE. 2013; 8:e53748. [PubMed: 23341992]

Pieperhoff S, Wilson KS, Baily J, de Mora K, Maqsood S, Vass S, Taylor J, Del-Pozo J, MacRae CA, Mullins JJ, Denvir MA. Heart on a plate: histological and functional assessment of isolated adult zebrafish hearts maintained in culture. PLoS ONE. 2014; 9:e96771. [PubMed: 24824845]

Porrello ER, Mahmoud AI, Simpson E, Hill JA, Richardson JA, Olson EN, Sadek HA. Transient regenerative potential of the neonatal mouse heart. Science. 2011; 331:1078–1080. [PubMed: 21350179]

Porrello ER, Mahmoud AI, Simpson E, Johnson BA, Grinsfelder D, Canseco D, Mammen PP, Rothermel BA, Olson EN, Sadek HA. Regulation of neonatal and adult mammalian heart regeneration by the miR-15 family. Proc. Natl. Acad. Sci. U.S.A. 2013; 110:187–192. [PubMed: 23248315]

Poss KD, Wilson LG, Keating MT. Heart regeneration in zebrafish. Science. 2002; 298:2188–2190. [PubMed: 12481136]

Raya A, Koth CM, Büscher D, Kawakami Y, Itoh T, Raya RM, Sternik G, Tsai H-J, Rodríguez-Esteban C, Izpisua Belmonte JC. Activation of Notch signaling pathway precedes heart regeneration in zebrafish. Proc. Natl. Acad. Sci. U.S.A. 2003; 100:11889–11895. [PubMed: 12909711]

Robinson MD, McCarthy DJ, Smyth GK. edgeR: a Bioconductor package for differential expression analysis of digital gene expression data. Bioinformatics. 2010; 26:139–140. [PubMed: 19910308]

Rogakou EP, Pilch DR, Orr AH, Ivanova VS, Bonner WM. DNA double-stranded breaks induce histone H2AX phosphorylation on serine 139. J. Biol. Chem. 1998; 273:5858–5868. [PubMed: 9488723]

Saretzki G, von Zglinicki T. Replicative aging, telomeres, and oxidative stress. Ann. N.Y. Acad. Sci. 2002; 959:24–29. [PubMed: 11976182]

Schnabel K, Wu C-C, Kurth T, Weidinger G. Regeneration of cryoinjury induced necrotic heart lesions in zebrafish is associated with epicar-dial activation and cardiomyocyte proliferation. PloS ONE. 2011; 6:e18503. [PubMed: 21533269]

Takeuchi T. Regulation of cardiomyocyte proliferation during development and regeneration. Dev. Growth Differ. 2014; 56:402–409. [PubMed: 24738847]

Tümpel S, Rudolph KL. The role of telomere shortening in somatic stem cells and tissue aging: lessons from telomerase model systems. Ann. N.Y. Acad. Sci. 2012; 1266:28–39. [PubMed: 22901253]

Wang J, Panáková D, Kikuchi K, Holdway JE, Gemberling M, Burris JS, Singh SP, Dickson AL, Lin Y-F, Sabeh MK, et al. The regenerative capacity of zebrafish reverses cardiac failure caused by genetic cardiomyocyte depletion. Development. 2011; 138:3421–3430. [PubMed: 21752928]

Wang J, Karra R, Dickson AL, Poss KD. Fibronectin is deposited by injury-activated epicardial cells and is necessary for zebrafish heart regeneration. Dev. Biol. 2013; 382:427–435. [PubMed: 23988577]

Willett CE, Cortes A, Zuasti A, Zapata AG. Early hematopoiesis and developing lymphoid organs in the zebrafish. Dev. Dyn. 1999; 214:323–336. [PubMed: 10213388]

Wright WE, Piatyszek MA, Rainey WE, Byrd W, Shay JW. Telomerase activity in human germline and embryonic tissues and cells. Dev. Genet. 1996; 18:173–179. [PubMed: 8934879]

Europe PMC Funders Author Manuscripts

Highlights

- Telomerase hyperactivation is an early event during zebrafish heart regeneration
- Telomerase loss of function impairs cardiac regeneration
- The proliferative response of cardiomyocytes is inhibited in *tert*$^{-/-}$ zebrafish
- Telomerase protects cardiac cells from DNA damage and limits cellular senescence

Europe PMC Funders Author Manuscripts

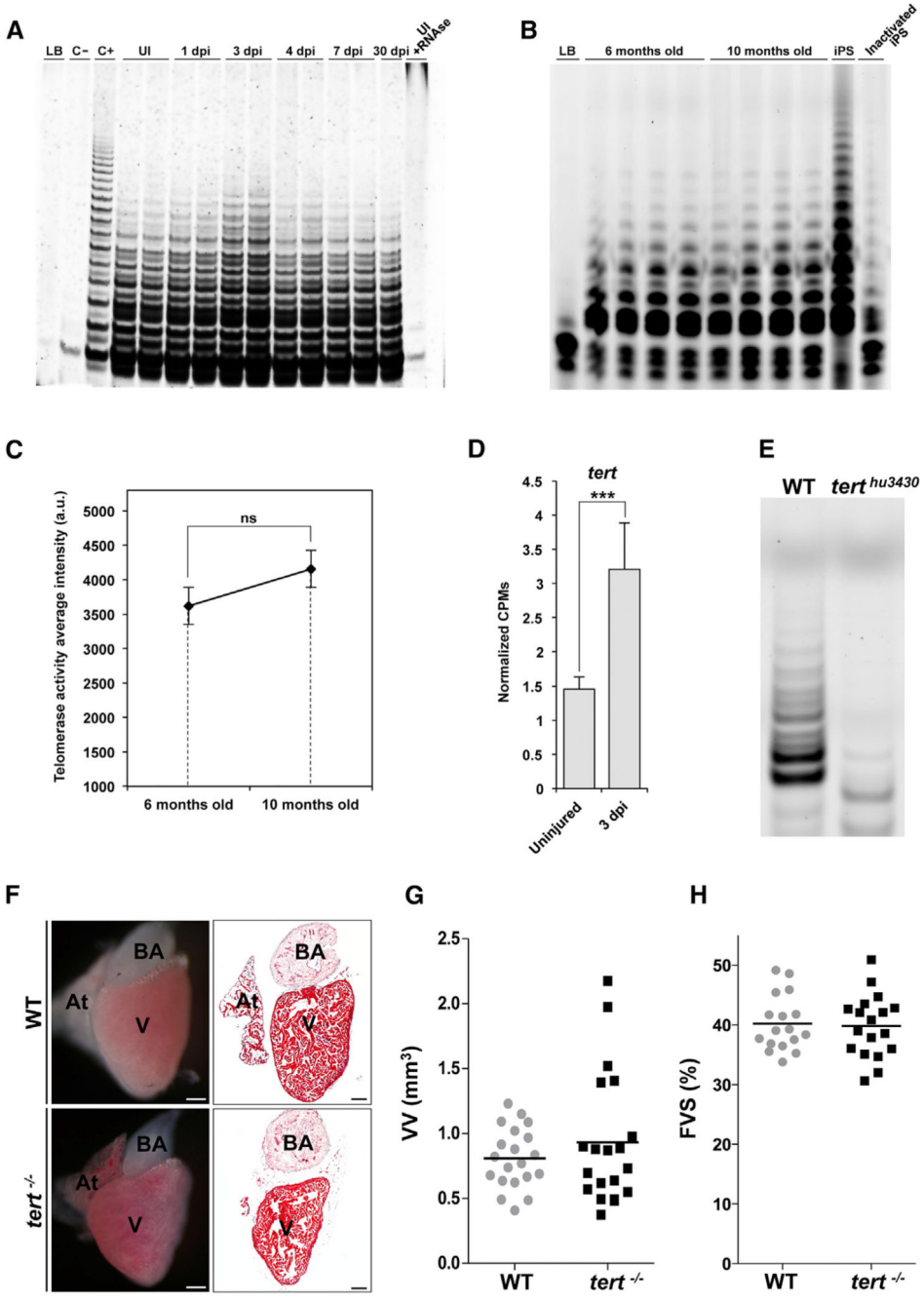

Figure 1. Heart Cryoinjury Augments Telomerase Activity and tert Expression Levels

(A) Representative telomeric repeat amplification protocol (TRAP) activity in uninjured (UI) hearts and hearts at 1, 3, 4, 7, and 30 days post cryoinjury (dpi) (n = 3/condition and time point). Positive control (C+), iPSCs; negative control (C−), *tert*$^{-/-}$ zebrafish heart; reaction specificity control, uninjured + RNase. LB, lysis buffer.

(B and C) Telomerase TRAP activity assay in 6- and 10-month-old zebrafish hearts (n = 4/time point). Data are means ± SEM. ns, not significant (unpaired Student's t test).

(D) Zebrafish *tert* mRNA expression levels in homeostasis and during regeneration (3 dpi) (n = 4 hearts/condition). CPMs, counts per million. Values are means ± SEM. ***p < 0.001 (B–H adjusted p value).

(E) Representative TRAP assay showing the lack of telomerase activity in $tert^{-/-}$ hearts (n = 3/genotype).

(F) Lack of telomerase does not affect heart development and function. There is normal anatomy and function in $tert^{-/-}$ zebrafish hearts. Shown are whole-mount views of dissected adult WT and $tert^{-/-}$ uninjured zebrafish hearts (left) and Masson-Goldner trichrome-stained sagittal sections (center). Five animals were analyzed per genotype. V, ventricle; At, atrium; BA, bulbus arteriosus. Scale bars, 100 μm.

(G and H) Echocardiographic evaluation of heart size (ventricular volume (VV) in diastole) (G) and cardiac function (ventricular FVS) (H) in uninjured WT and $tert^{-/-}$ animals. Values for both parameters did not differ between genotypes. Circles and squares show data for individual animals. Horizontal bars represent the mean (unpaired Student's t test). A total of 17–20 animals were analyzed per genotype.

Europe PMC Funders Author Manuscripts

Europe PMC Funders Author Manuscripts

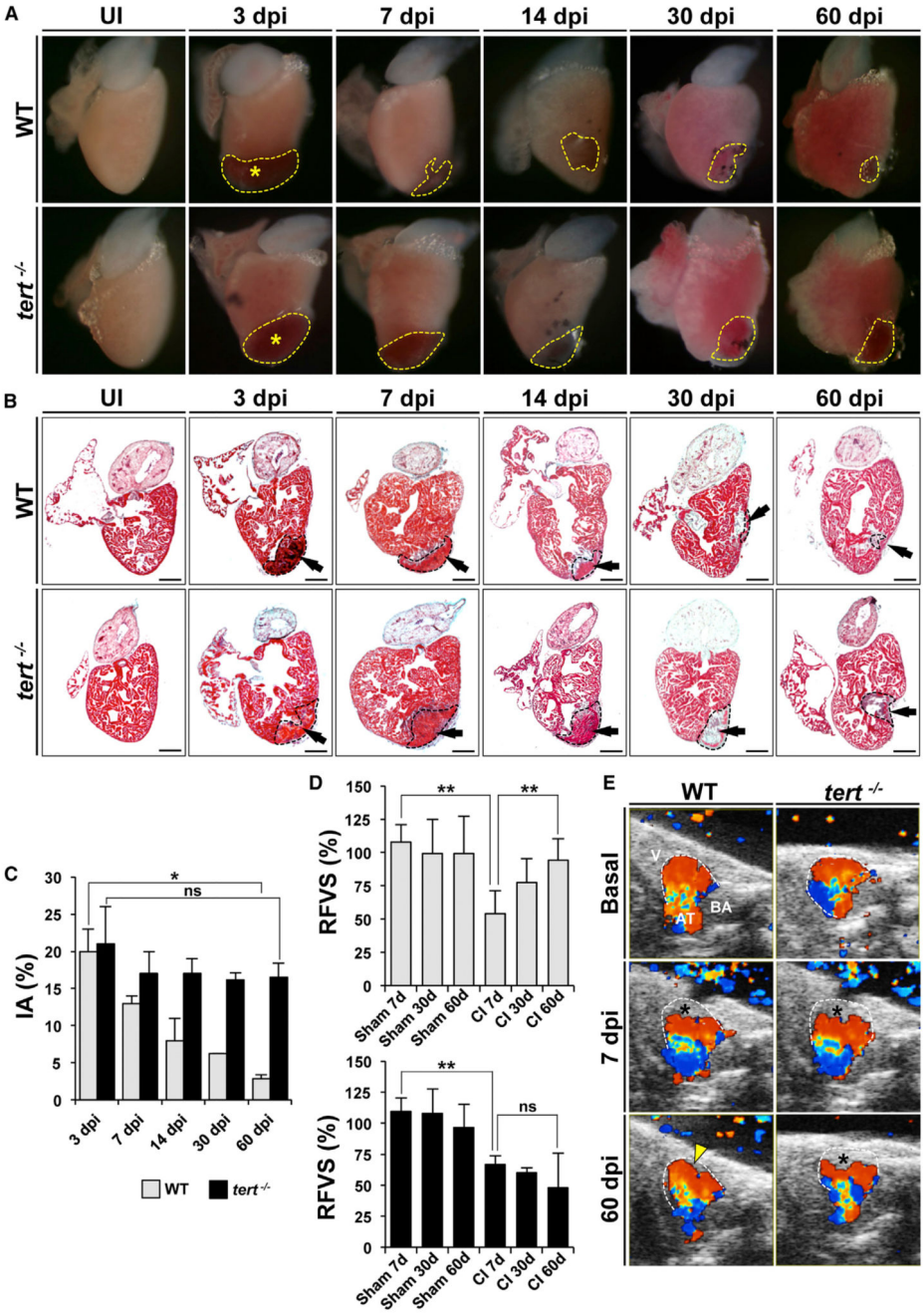

Figure 2. Heart Regeneration Is Inhibited Strongly in tert$^{-/-}$ Animals

(A) Whole-mount views of uninjured and cryoinjured WT and *tert*$^{-/-}$ zebrafish hearts dissected at the indicated times post-injury. Dotted lines outline the injured area. Asterisks mark the initial injury site.

(B) Masson-Goldner trichrome staining of sagittal sections of uninjured WT and *tert*$^{-/-}$ hearts at the indicated days after cryoinjury. Dotted black lines outline the injured area. Arrows mark the initial injury site. Scale bars, 100 μm.

(C) Size of the ventricle injury (injured area [IA]) on sagittal heart sections at the indicated times post-injury, presented as the percentage of the total ventricular area. Data are means of at least 4 sections/heart from 3-8 hearts/time point, with the exception of WT 30 dpi, where only one heart was analyzed. Data are means ± SEM. *p < 0.05 (Mann-Whitney test).
(D) Relative FVS (RFVS) in WT and *tert*$^{-/-}$ zebrafish hearts under the basal condition (sham-operated animals) and at the indicated times post-injury. WT hearts recover ventricular function over time but *tert*$^{-/-}$ hearts do not. Data are means ± SEM of a pool of 10 animals/condition. **p < 0.01 (one-way ANOVA followed by Tukey's honest significant difference test).
(E) Representative Doppler echocardiography images of intracardial blood flow in WT and *tert*$^{-/-}$ hearts in the absence of injury and at the indicated times post-injury. Asterisks mark the initial injury site. See also Movies S1, S2, S3, S4, S5, and S6.
See also Figures S1–S3, and Table S1.

Europe PMC Funders Author Manuscripts

Europe PMC Funders Author Manuscripts

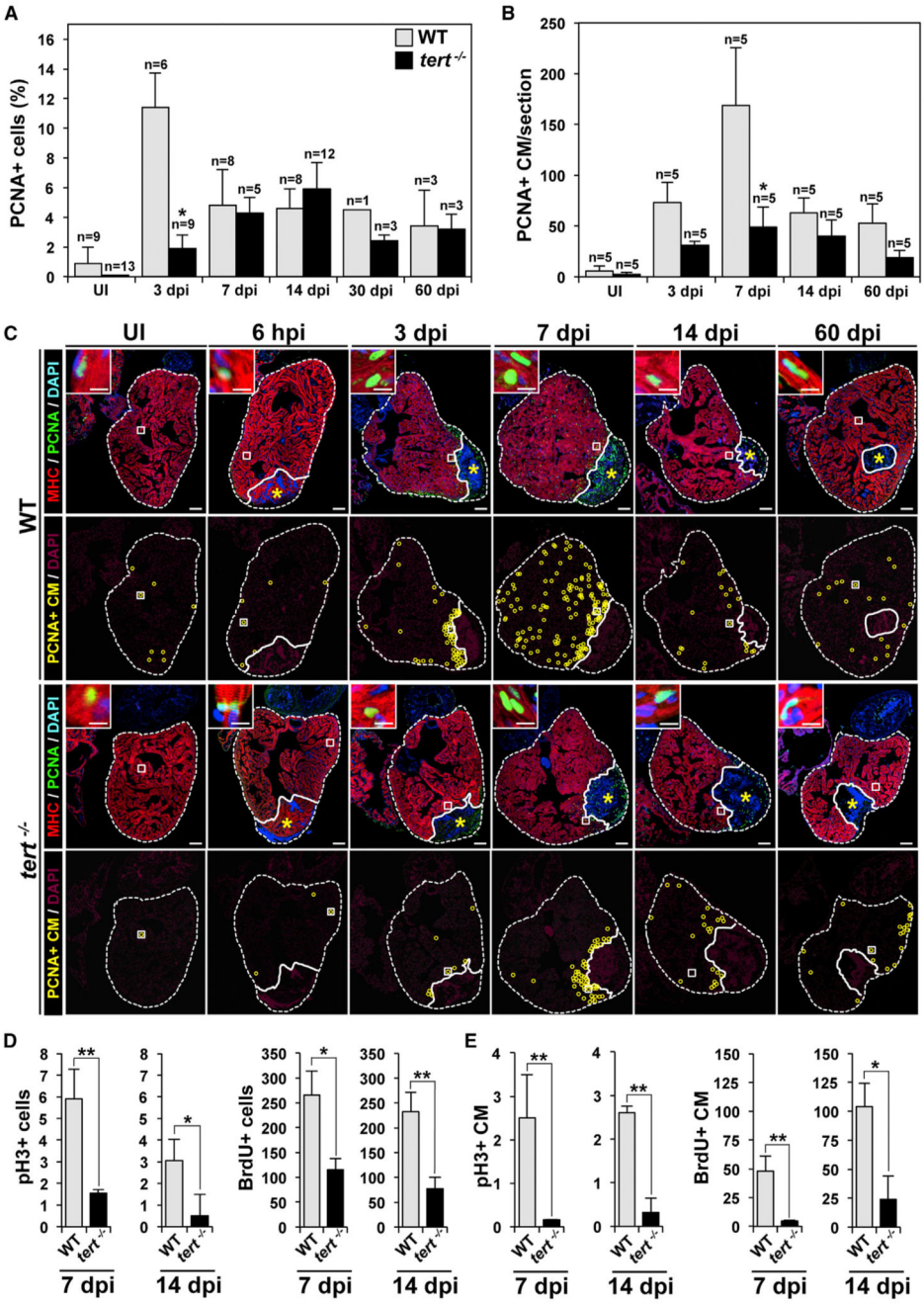

Figure 3. The Absence of Telomerase Severely Affects Cardiomyocyte Proliferation

(A and B) Cardiac cells positive for PCNA in UI WT and *tert*$^{-/-}$ zebrafish hearts and in hearts at the indicated days after cryoinjury. (A) PCNA^{+} total cardiac cells. (B) PCNA^{+} cardiomyocytes. Data are means ± SEM of the percentage of PCNA^{+} cells (A) or number of PCNA^{+} cardiomyocytes per cardiac ventricle section (at least 3 sections/animal from the indicated number of animals) (B). *$p < 0.05$ compared with WT samples (Mann-Whitney test).

(C) WT and *tert*$^{-/-}$ heart sections immunostained with anti-MHC to mark cardiomyocytes (red) and anti-PCNA to mark cells in S phase (green). Nuclei were counterstained with DAPI (blue). The bottom rows show the location of PCNA^{+} cardiomyocytes during regeneration (yellow circles). The nuclear area is shown in magenta. Dotted lines outline the ventricle and injured area. Asterisks mark the initial injury site. Insets show high-magnification views of representative PCNA^{+} cardiomyocytes in the boxed areas. Scale bars, 100 μm (whole-heart views) and 10 μm (magnifications).

(D and E) Quantification of pH3^{+} and BrdU-labeled cardiac cells (D) and cardiomyocytes (E) at 7 and 14 dpi. Data are means ± SEM. *$p < 0.05$, **$p < 0.01$ (unpaired Student's t test).

See also Figures S4 and S5.

Europe PMC Funders Author Manuscripts

Europe PMC Funders Author Manuscripts

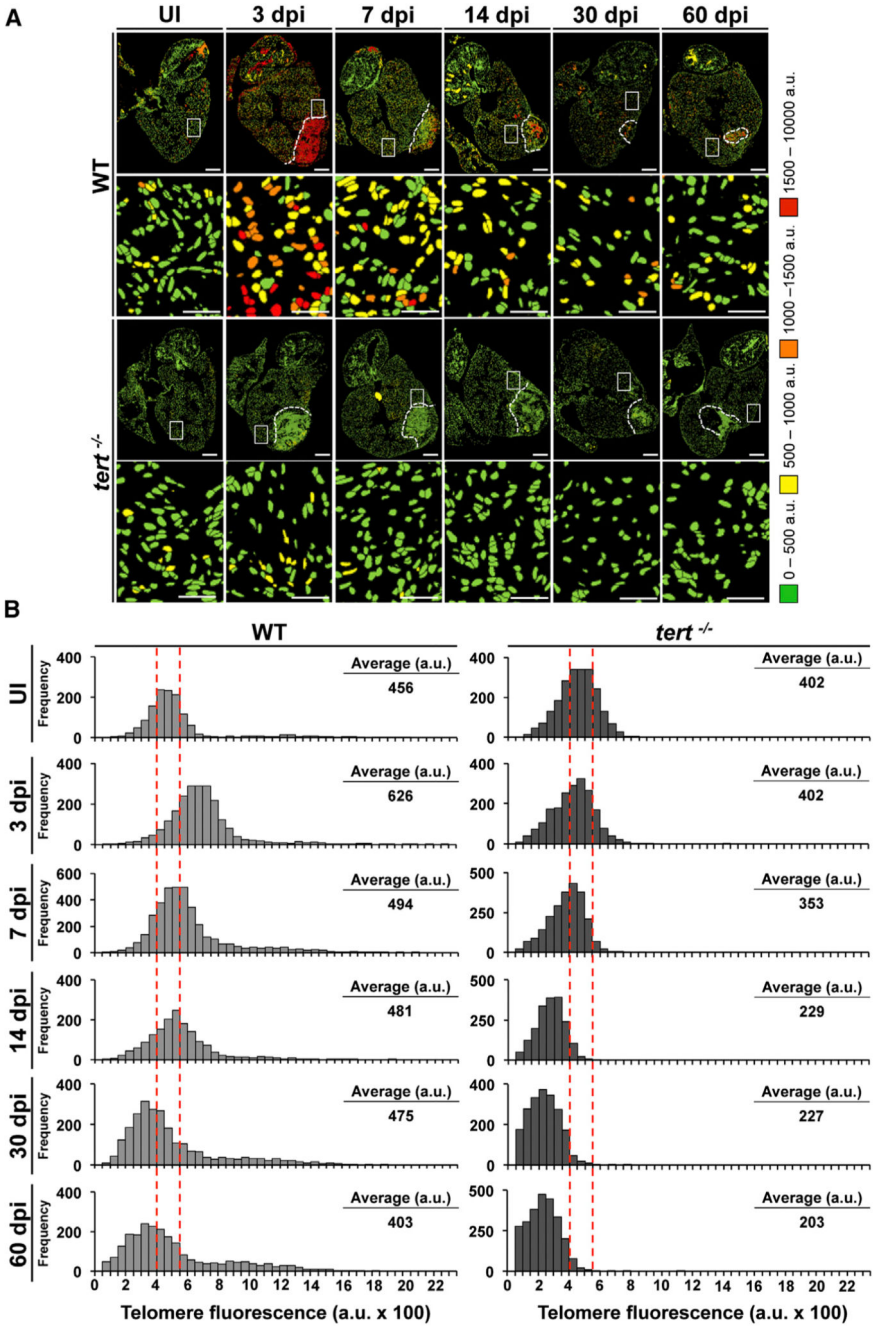

Figure 4. Heart Cryoinjury Induces a Telomerase-Dependent Increase in Telomere Reserves

(A) Representative telomap images of WT and tert$^{-/-}$ heart, uninjured (UI) or fixed at different days postinjury [dpi]. Nuclei are assigned a four-color code according to their average telomere fluorescence in a.u. The cells with the longest telomeres are visualized in red, and the cells with the shortest telomeres are presented in green. Dotted lines mark the injured area. The second and fourth rows show higher magnifications of the boxed areas highlighted in the entire heart section images. Scale bars, 100 μm and 10 μm for magnification images.

(B) Telomere fluorescence frequency histograms of cardiac WT and *tert*$^{-/-}$ cells in uninjured hearts and hearts at 3, 7, 14, 30, and 60 days after cryoinjury. Mean telomere fluorescence is indicated in a.u. The injury site was excluded from the analysis. Note the increase in the number of cells with long telomeres at 3 dpi in WT hearts, followed by reestablishment of the initial profile. This response is lacking in *tert*$^{-/-}$ cells, and, at later stages, cells have shorter telomeres than initially. See also Figure S6.

Europe PMC Funders Author Manuscripts

Europe PMC Funders Author Manuscripts

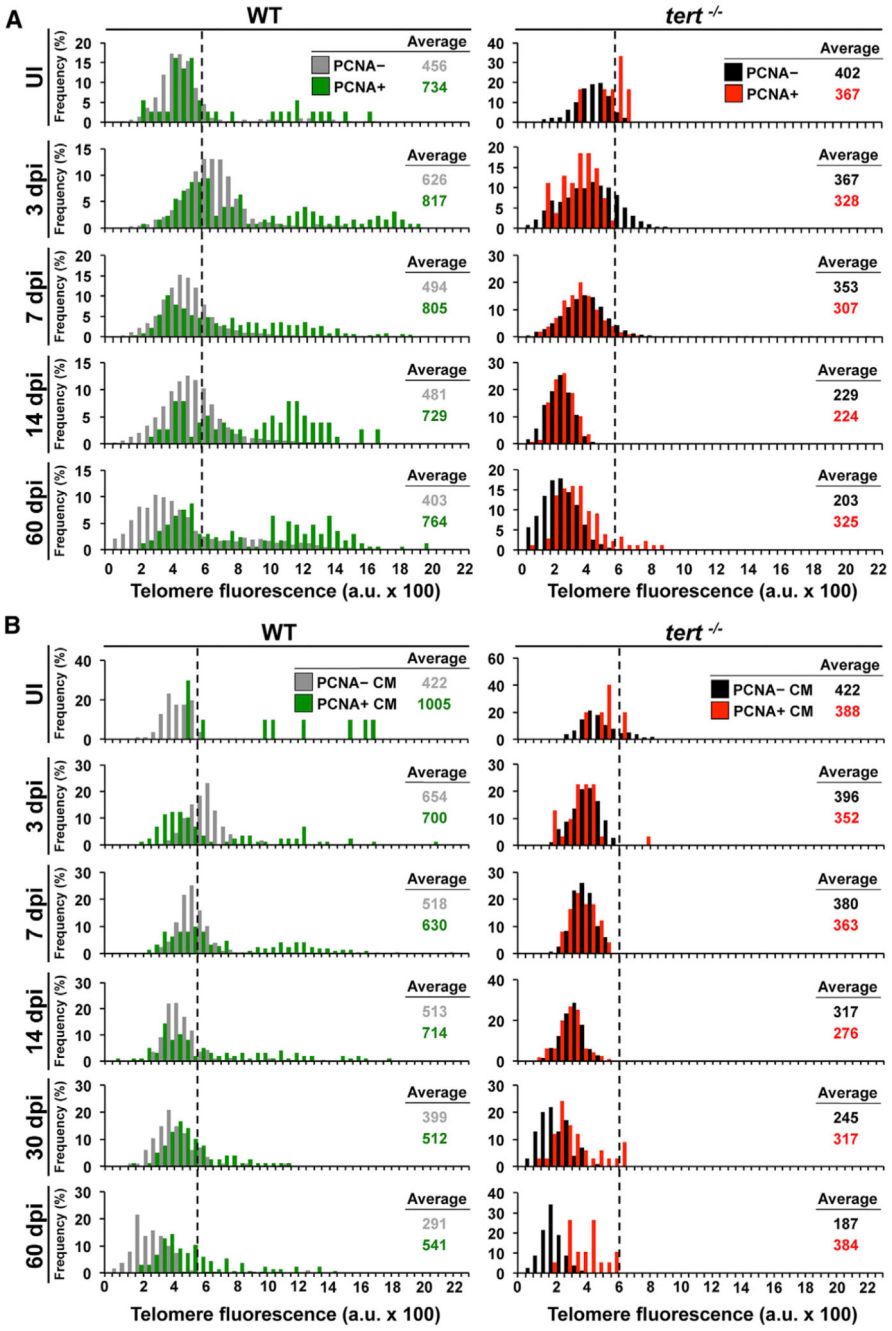

Figure 5. Long Telomeres Mark a Subset of Proliferating Cardiac Cells, Including Proliferating Cardiomyocytes

(A and B) Telomere fluorescence frequency histograms of PCNA^{-} and PCNA^{+} WT and *tert*$^{-/-}$ cells in uninjured hearts and hearts at 3, 7, 14, 30, and 60 days after cryoinjury. Histograms show frequencies for (A) total cardiac cells and (B) cardiomyocytes. Telomere fluorescence averages are indicated in a.u. Note that in both cases the subpopulation of proliferating cells with long telomeres is lacking in *tert*$^{-/-}$ hearts. CM, cardiomyocytes. See also Figure S6.

Europe PMC Funders Author Manuscripts

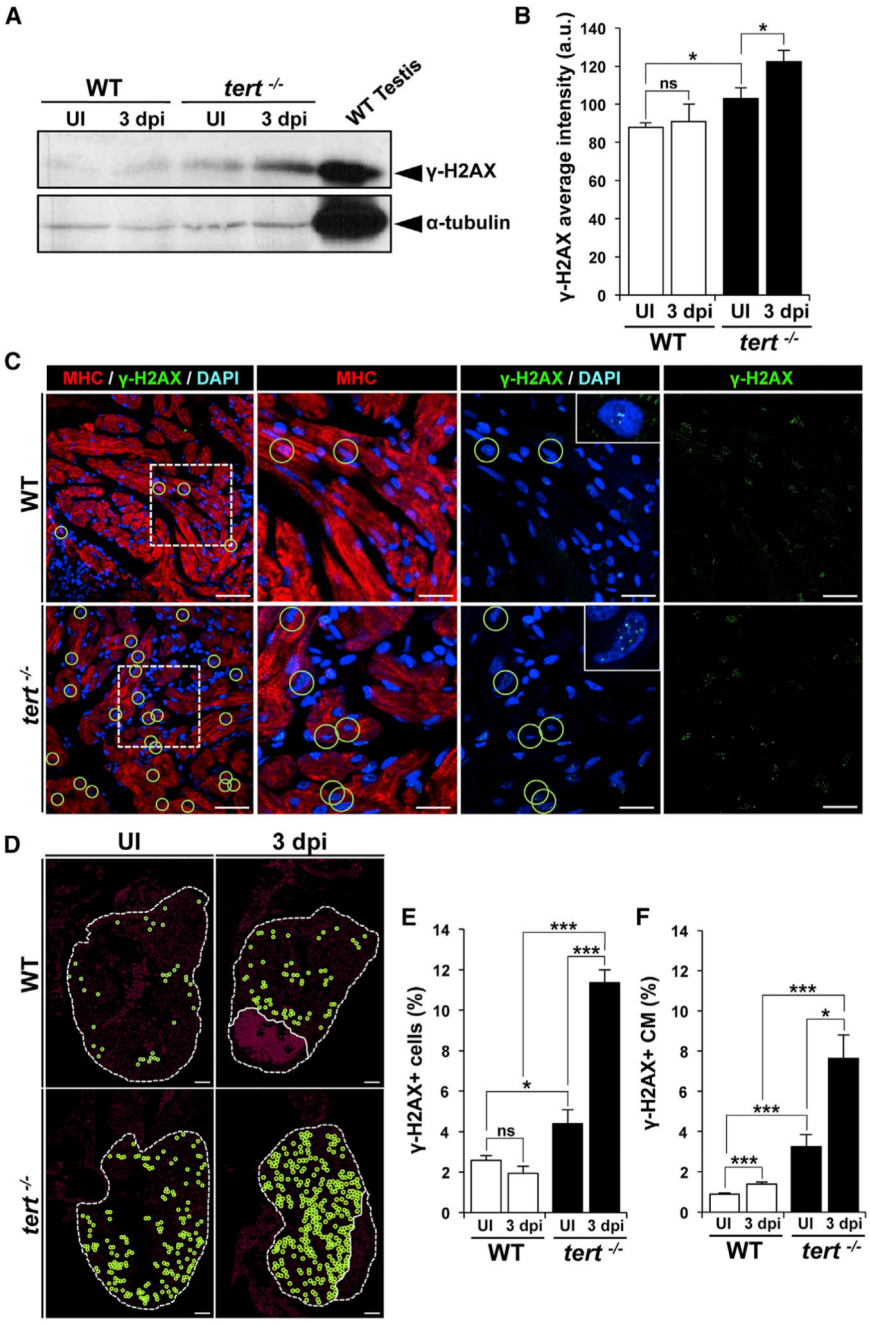

Figure 6. DNA Damage Increases Strongly after Ventricular Cryoinjury in the Absence of Telomerase

(A) Representative western blot of γ-H2AX expression in WT and *tert*$^{-/-}$ hearts without injury and in hearts at 3 dpi.

(B) Quantification of western blot signal intensities (n = 9 hearts/condition). Data are means ± SEM. *p < 0.05 (Mann-Whitney test).

(C) Representative staining of γ-H2AX foci (green) in cardiac cells in uninjured and 3 dpi WT and *tert*$^{-/-}$ hearts. Cardiomyocytes are immunostained with anti-MHC (red), and nuclei

are counterstained with DAPI (blue). Examples of γ-H2AX^{+} cardiomyocytes are outlined with green circles. Boxed areas are shown at a higher magnification. Scale bars, 20 μm.
(D) Distribution of γ-H2AX-positive cardiomyocytes (green circles) in uninjured and 3 dpi WT and *tert*$^{-/-}$ hearts. The nuclear area is shown in magenta. The ventricle and injured area are outlined by dotted lines. Scale bars, 100 μm.
(E and F) Percentages of (E) γ-H2AX-positive cardiac cells and (F) γ-H2AX-positive cardiomyocytes in uninjured and 3 dpi WT and *tert*$^{-/-}$ hearts. Data are means ± SEM of cells counted on a minimum of 3 sections/heart in four hearts. *$p < 0.05$, **$p < 0.01$, ***$p < 0.001$ (Student's t test). See also Figure S7.

Europe PMC Funders Author Manuscripts

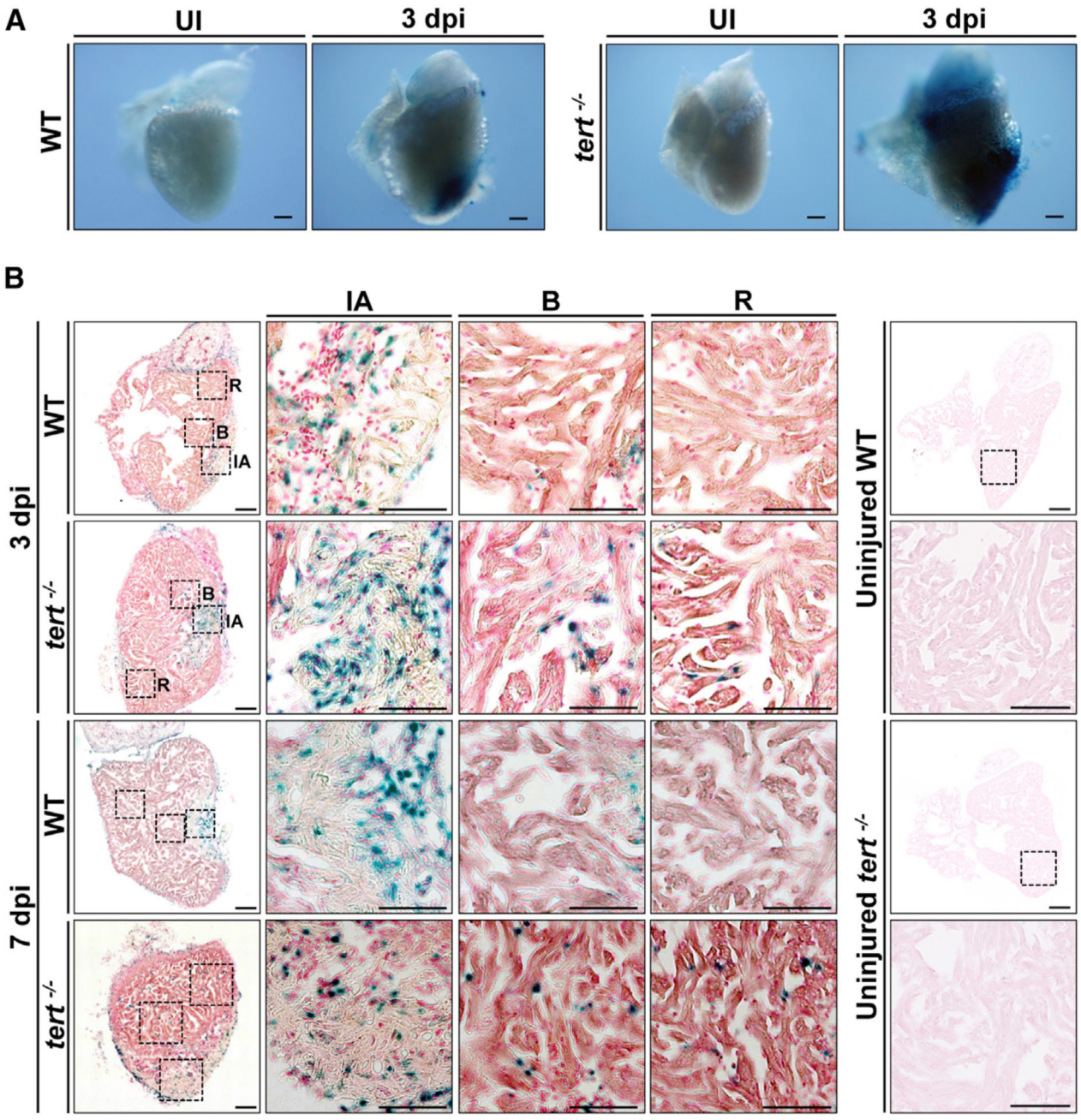

Figure 7. tert$^{-/-}$ Hearts Acquire a Senescence Phenotype after Ventricular Cryoinjury

(A) Whole mounts of uninjured and 3 dpi WT and *tert*$^{-/-}$ hearts stained for SA β-galactosidase. Scale bars, 100 μm.

(B) Cryosections of uninjured, 3 dpi, and 7 dpi WT and *tert*$^{-/-}$ hearts stained for SA β-galactosidase. Magnified views are shown of the injured area, injury border (B), and remote zone (R). Scale bars, 100 μm (whole heart) and 50 μm (magnified views).